# Coulomb stress transfer and fault interaction over millennia on non-planar active normal faults: the Mw 6.5-5.0 seismic sequence of 2016-2017, central Italy.

Zoe K. Mildon[1.], Gerald P. Roberts[2.], Joanna P. Faure Walker[1.], Francesco Iezzi[2.]

1. Institute for Risk and Disaster Reduction, University College London, Gower Street, London, WC1E 6BT, UK

2. Department of Earth and Planetary Sciences, Birkbeck, University of London, Malet Street, London, WC1E 7HX, UK

**Abstract**

In order to investigate the importance of including strike-variable geometry and the knowledge of historical and paleoseismic earthquakes when modelling static Coulomb stress transfer and rupture propagation, we have examined the August-October 2016 and January 2017 central Apennines seismic sequence (Mw 6.0, 5.9, 6.5 in 2016 (INGV) and Mw 5.1, 5.5, 5.4, 5.0 in 2017 (INGV). We model both the coseismic loading (from historical and paleoseismic earthquakes) and interseismic loading (derived from Holocene fault slip-rates) using strike-variable fault geometries constrained by fieldwork. The inclusion of the elapsed times from available historical and paleoseismological earthquakes and on faults enables us to calculate the stress on the faults prior to the beginning of the seismic sequence. We take account of the 1316-4155 years elapsed time on the Mt. Vettore fault (that ruptured during the 2016 seismic sequence) implied by paleoseismology, and the 377 years and 313 years elapsed times on the neighbouring Laga and Norcia faults respectively, indicated by the historical record. The stress changes through time are summed to show the state of stress on the Mt. Vettore, Laga and surrounding faults prior to and during the 2016-

2017 sequence. We show that the build up of stress prior to 2016 on strike-variable fault geometries generated stress heterogeneities that correlate with the limits of the mainshock ruptures. Hence we suggest that stress barriers appear to have control on the propagation and therefore the magnitudes of the mainshock ruptures.

**Keywords**: Earthquake interaction, forecasting, and prediction; dynamics and mechanics of faulting; Continental tectonics: extensional; mechanics, theory, and modelling; Europe; palaeoseismology

## 1. Introduction

The 2016-2017 seismic sequence of central Italy began on the 24th August at 03:36 with a Mw 6.0 earthquake (Event 1, magnitude from the INGV) occurring close to the town of Amatrice. This earthquake caused the destruction of many small towns in the region and 297 deaths. Numerous aftershocks were recorded in the following weeks, which followed an Omori-type decay [*Peruzza et al.*, 2016]. The decay was interrupted on the 26th October by two earthquakes that occurred in quick succession (19:10 and 21:18 (Event 2) local time, Mw 5.4 and 5.9 respectively, magnitude from the INGV) to the north, centred on the town of Visso. No deaths were reported, but there was further damage to buildings in the region. The largest earthquake in the sequence occurred on the 30th October at 08:40, Mw 6.5 (Event 3, magnitude from the INGV) between and re-rupturing the locations of the 24th August and 26th October events (Figure 1). Three indirect deaths were reported, but buildings experienced further serious damage, including the collapse of the San Benedetto basilica in Norcia. The time since the 18th January 2017 has been marked by the occurrence of further seismicity in the SE of the epicentral area including events of Mw 5.1, 5.5,

5.4, 5.0 (magnitudes from the INGV) which may have indirectly triggered an avalanche that resulted in a further 29 deaths.

The two previous large (≥Mw 6.0) earthquakes in this region prior to 2016 occurred to the north-west (1997 Umbria-Marche seismic sequence, Cello *et al.* [1998], Vittori *et al.* [2000]) and the south-east (2009 L'Aquila earthquake, Alessio *et al.* [2009], Chiaraluce *et al.* [2010]). The mainshocks (with focal mechanisms) and aftershocks from these three events are shown in Figure 1. These events both occurred along strike of the location of the 2016-2017 seismic sequence, leading to discussion of the possibility that the 2016 seismicity filled a seismic gap [*Stein and Sevilgen*, 2016] with both the 1997 and 2009 events increasing the stress in the 2016 epicentral area [*Nostro et al.*, 2005; *Walters et al.*, 2009]. If this region is a seismic gap, we are interested in why the pattern of mainshocks began in the south, jumped to the north, and then finally ruptured in between the two previous 2016 mainshocks. In this paper we only consider the static stress transfer during the sequence, as the time between the earthquakes is probably too long to be due to dynamic stress transfer.

In particular, we have calculated the static Coulomb stress changes [*Harris and Simpson*, 1992; *Reasenberg and Simpson*, 1992] leading up to and during the 2016 seismic sequence on faults with strike-variable geometry. We add additional information to the discussion of the possible seismic gap: the elapsed times since previous large magnitude earthquakes on the Laga, Mt. Vettore and Norcia faults and modeling of all coseismic events and interseismic loading since 1349 A.D.. We emphasise that the Mt. Vettore fault most likely had the longest elapsed time in the region, and hence, presumably, the highest accumulated stress at depth. We also

emphasise that the accumulated stress on the Mt. Vettore fault prior to 2016 was most-likely non-uniform, due to the spatial distribution of historical events and its strike-variable geometry. We discuss whether such stress heterogeneity on the Mt. Vettore fault represented a stress barrier, such as those that have previously been hypothesised to limit the area of fault that ruptures during earthquakes [*Steacy and McCloskey*, 1998; *Rydelek and Sacks*, 1999]. We suggest that stress heterogeneities may be used to explain the sequence and limits of the three mainshocks that occurred during the 2016 seismic sequence.

## 2. Method

The surface traces of active normal fault scarps in Figure 1 and subsequent figures are part of an active fault database compiled in Google Earth™ based on extensive fieldwork (>14,000 slip vector and fault orientation measurements at >800 sites, from Morewood and Roberts [2000]; Roberts and Michetti, [2004]; Papanikolaou *et al.* [2005]; Papanikolaou and Roberts [2007]; Roberts [2008]; Faure Walker *et al.* [2010], [2012]; Wilkinson *et al.* [2015]; Mildon *et al.* [2016a]), satellite imagery (Google Earth™), paleoseismology studies (e.g. Galli *et al.* [2008]) and geological maps. The locations of these faults are constrained to within a few tens of metres and the strike and dip of these fault are known to ~±5$^{o}$ accuracy. These uncertainties do not greatly affect the generation of strike-variable fault planes and subsequent modelling of Coulomb stress transfer. It has been shown that the faults that have been mapped are sufficient to accommodate most or all of the tectonic strain across the width of the Apennines because strains implied by fault scarps that have formed since 15 ±3 ka match those from GPS when summed across the width of the Apennines [*Faure Walker et al.*, 2010] and correlate with large-scale features such as orogen-wide

topography, total throws (vertical component of the slip) across the faults and SKS splitting delay times in the underlying mantle [*Faure Walker et al.*, 2012; *Cowie et al.*, 2013]. Other minor structures may also exist with little or no geomorphic expression; we do not include such features in our modelling. The traces of the active fault scarps we include are used to build 3D fault planes comprised of numerous rectangular elements with strike variable geometry and a constant value of dip. This is a 1$^{st}$ order approximation, because the fault geometry could change at depth, but few data constrain this. The dip that we use for each fault is determined from field measurements or from the literature (e.g. Boncio *et al.* [2004], Pace *et al.* [2006]). The size of elements used is 1km; this is a trade-off between observations and computational time. The strike-variable geometry is defined by field measurements [*Roberts and Michetti*, 2004; *Roberts*, 2007; *Faure Walker et al.*, 2009, 2010; *Wilkinson et al.*, 2015; *Mildon et al.*, 2016a]. Faults are assumed to project to depth perpendicular to the overall strike of the fault, maintaining a cylindrical geometry, and short faults are assumed to maintain an aspect ratio of 1. Again, this is a 1$^{st}$ order approximation, because the fault geometry could change at depth, but few data constrain this. The thickness of the seismogenic zone and brittle faulting is assumed to be 15 km [*Cowie et al.*, 2013]. This method is outlined in more detail in Mildon *et al.* [2016c]. Ductile shear zones are modelled to be projections of the brittle faults from 15-24 km depth. Stress changes between the strike-variable faults generated using this method are calculated in *Coulomb 3.4* [*Lin and Stein*, 2004; *Toda et al.*, 2005], which uses an elastic half space model.

## 2.1 Interseismic modelling

To model the interseismic loading of the active normal faults in the upper crust, ductile shear zones are modelled directly down-dip of the brittle portion of the faults [*Wedmore et al.*, 2015, submitted.; *Wedmore*, 2017]. The shear zones are modelled as slipping incrementally and transferring Coulomb stress to the base of the brittle upper portions of the faults. The rate of slip on the shear zones equals the rate of post 15 ± 3 ka slip measured in the field across the active bedrock scarps exposed at the surface [*Roberts and Michetti*, 2004; *Papanikolaou et al.*, 2005; *Papanikolaou and Roberts*, 2007; *Faure Walker et al.*, 2009, 2010; *Wilkinson et al.*, 2015; *Mildon et al.*, 2016a] and new throw measurements presented herein (Figure 2), following the mechanical model advocated by Cowie *et al.* [2013]. The post 15 ± 3 ka slip-rates measured at the surface are assumed to be representative of the long-term as the scarps are formed over numerous seismic cycles. When summed across strike, the surface throws and the strain-rates they imply correlate with total throws, SKS splitting in the mantle and long wavelength topography [*Faure Walker et al.*, 2012; *Cowie et al.*, 2013]. A cross section illustrating this model set up and the resulting stress pattern is shown in Figure 2b. The interseismic slip distribution is constructed by linearly interpolating between the values of slip measured at the surface and zero at the tips of the faults. The rake is assumed to be $-90^{o}$ for the entire extent of the shear zone. It is assumed that the shear zones have the same dip, and are direct continuations of the upper brittle portions of the faults. Again, this is a $1^{st}$ order approximation, because the shear zone geometry could change at depth, but few data constrain this.

To illustrate how post 15 ± 3 ka slip-rates are determined we present examples of profiles across fault scarps in Figure 2. The profiles are constructed using chain-surveying techniques using steel-rules and clinometers, and a number of sites are

checked with barometric altimeters and tripod-based LiDAR (e.g.Wilkinson *et al.* [2015]). In particular we note during field work the position of the upper slope, the degraded free face, the preserved free face, the colluvial wedge and the lower slope (see Papanikolaou *et al.* [2005] for further information). This information is used to construct the profiles and to interpret the Holocene throw. Scarps show natural variability in offset along strike and our experience of multiple scarp profiles (e.g.Wilkinson *et al.* [2015]) leads us to assign an error of ± 20% to the throw values. The throw since 15 ±3 ka on the Mt. Vettore fault used herein is 5.20 ± 1.04 m close to the centre of the fault (Figure 2c). The throw on the Laga fault used herein is 9.82 ± 1.96 m close to the centre of the fault (Figure 2d). The expression of the Norcia fault is less clear in the field as there is little well developed and exposed Holocene bedrock scarp. Hence using the relationship between fault length and post 15 ±3 ka throw from forty-eight other faults in the Apennines [*Roberts and Michetti*, 2004; *Papanikolaou et al.*, 2005; *Papanikolaou and Roberts*, 2007; *Faure Walker et al.*, 2009, 2010, 2012; *Wilkinson et al.*, 2015; *Mildon et al.*, 2016a], a throw of 11.9 m is assigned to the Norcia fault. This value will have a higher error due to the spread in data; hence an error of 50 % has been assigned. This gives slip rates of 0.35 ± 0.1 mm/yr, 0.65 ± 0.13 mm/yr and 0.79 ± 0.43 mm/yr for the Mt. Vettore, Laga and Norcia faults respectively. These values are within error of values reported from paleoseismology [*Galadini and Galli*, 2000].

With regard to the time over which interseismic loading should be applied to each fault, we utilise information from the historical record and paleoseismology. The historical record is thought to be complete for events > Mw 5.8 since 1349 A.D. [*Michetti et al.*, 1996] due to shaking records made by scholars through history and

compiled in the CFTI catalogue [*Guidoboni et al.*, 2007]. The last earthquake > Mw 6.0 on the Norcia fault was in 1703 A.D. [*Blumetti*, 1995; *Galli et al.*, 2005], giving an elapsed time of 313 years. On the Laga fault, the last earthquake was in 1639 A.D. [*Pace et al.*, 2002; *Guidoboni et al.*, 2007], giving an elapsed time of 377 years. On the Mt. Vettore fault, there is no known earthquake in the historical catalogue that can be associated with this fault, even prior to 1349 A.D. The elapsed time is determined from paleoseismic trenching to be in the range of 1316-4155 years B.P. [*Galadini and Galli*, 2003].

2.2 Coseismic modelling

We have modelled thirty-four earthquakes with > Mw 5.5 from 1349 A.D. to 2016 A.D. and calculated the coseismic stress changes resolved onto all the surrounding active faults for the central Apennines. Detailed slip distribution information is not available for these pre-instrumental earthquakes hence we have used simple linear slip gradients to produce concentric slip distributions. Assuming a triangular slip profile at the surface (following from field data presented in [*Roberts*, 2007]) and a triangular slip profile with depths produces a concentric slip distribution. At the time of writing no non-preliminary slip-distributions have been published for the 2016-2017 sequence based on modelling InSAR so we have also used so again we use simple linear slip gradients (although see below for more detail). We also note that such modelling tends to use simplified planar fault geometries, so we would be unable to directly apply them onto the non-planar faults we have measured in the fault and modelled, another reason why we have used simple linear slip gradients. The rupture length used to define the dimensions of the slip distribution is calculated from the magnitude of the event in the CFTI catalogue, using the relationship presented in Wells and

Coppersmith [1994]. If the calculated rupture length is shorter than the assigned fault that ruptures, then the location of the slip along the responsible fault is inferred from the distribution of shaking [*Guidoboni et al.,* 2007]. Paleoseismic records are also used to help constrain which fault and how much of that fault ruptures (e.g. Galadini and Galli [2003]; Galli *et al.* [2008]). The distribution and dates of historical ruptures since 1349 A.D. is shown in Figure 1.

In addition to the historical ruptures in the CFTI catalogue, the three largest earthquakes in 2016 and the four Mw>5.0 earthquakes that occurred on the 18$^{th}$ January 2017 have been modelled to determine the evolution of Coulomb stress during the sequence. For Event 1 (24$^{th}$ August), a slip distribution based on one released by the INGV, that is determined through preliminary modelling of InSAR fringes and observations of surface ruptures with ~20 cm maximum surface offset throw [*Livio et al.*, 2016], has been used to model the coseismic stress changes [*INGV working group*, 2016]. For Event 2 (26$^{th}$ October), no slip distribution has been published at the time of writing, so a simple concentric slip distribution has been used. This may well be consistent with the relatively simple concentric structure of the InSAR fringes for this event [*COMET*, 2016]. To deduce the length of fault that ruptured, we measured the distance covered by the InSAR fringes parallel to the mean fault strike; this distance was 13 km. A simple concentric slip distribution was used, with zero slip at the edges of the fault and at 11 km depth. The depth of the rupture is based on the width of the fringes, which were comparable to Event 1. A maximum slip of 0.58m in the center of the fault was chosen to agree with the published moment magnitude from the USGS. Surface faulting was observed during this event of a few centimetres to decimetres (A. Michetti *pers. comm.*) hence we include this in the

model such that surface slip is 10 % of the maximum slip at depth (based on relationships of slip at depth and at the surface from historical and recent earthquakes; Wells and Coppersmith [1994]). For Event 3 (30th October), no slip distribution has been published at the time of writing; hence a simplified concentric slip distribution is also used. The slip distribution has the location of maximum slip skewed to the south-east and located directly down dip of the observed location of maximum surface slip [*Mildon et al.*, 2016b]. To a first order approximation, this is likely to be consistent with unpublished InSAR fringes [*COMET*, 2016] which appear to be skewed and more numerous to the south-east. It is assumed that the whole of the Mt. Vettore fault ruptured during Event 3, based on the observations of surface ruptures and the extent of the InSAR fringes [*Iezzi et al., in prep.*]. Again, the maximum slip of 2.05 m was chosen to agree with the published moment magnitude. We acknowledge that these are simplified slip distributions. However, published slip distributions for other recent earthquakes in Italy are non-unique (e.g. see Wilkinson *et al.* [2015]) and are most commonly generated assuming a planar geometry. Hence we have taken the most prominent features of the available information (InSAR fringes and surface observations) to generate the simplified slip distributions we have used on strike-variable faults, and this could be improved in future iterations.

The four earthquakes that occurred on the 18th January 2017 (Mw 5.1, 5.5, 5.4, 5.0) can be related to the Laga fault, based on their location. No published slip distributions or INSAR results are available. The stress change associated with these events has been included, despite their small magnitude. Using the magnitude for each event, the rupture area was calculated based on Wells and Coppersmith [1994]. A rectangular or square rupture area was used for each event and a concentric slip

distribution assigned. The rupture dimensions and maximum slip used are 3x4 km & 0.35 m, 6x5km and 0.6 m, 5x5 km and 0.41 m and 3x3 km and 0.28 m respectively. The location of the patches of the Laga fault that slips is assigned based on earthquake locations provided by the INGV.

### 2.3 Cumulative transferred stress

In order to determine the stress history on the faults of interest, the interseismic and coseismic Coulomb stress transfer onto the brittle portions of the active faults are summed together over time. This summation is done for each individual element of the gridded strike-variable faults. As a starting point, we assume that the stress on all the faults was zero in 1349 A.D., as this is the time from when the historical record for Mw > 5.8 is considered complete. This approach has been adopted following previous studies [*Deng and Sykes*, 1997; *Nalbant et al.*, 1998]. However we also calculate the stress for the Mt. Vettore, Norcia and Laga faults implied by the elapsed times from paleoseismology and the historical record, which in the case of the Mt. Vettore fault could extend back to 4155 years B.P. We assume that following an earthquake, the Coulomb stress on the portion of the fault that slips drops essentially to zero. While this is likely a simplification, the stress must drop to close to zero, especially in the largest earthquakes, otherwise there would be a large accumulation of stress over many seismic cycles, which is unrealistic. Some off-fault deformation may also occur to relieve stresses, however in contrast to the stress drop experienced by the fault that ruptures, the magnitude of this stress relieved is likely to be much smaller.

## 3. Results

### 3.1 Interseismic loading

The Coulomb loading rate from interseismic slip across the shear zones at depth has been calculated for all the faults, and shown in detail for the Mt. Vettore, Laga and Norcia faults. These three faults are the main seismogenic structures in the region of interest, in the so-called seismic gap between the 1997 and the 2009 seismic sequences. The pattern of interseismic stress transferred to the upper brittle portions of the faults for one year is shown in Figure 2. The mean values of Coulomb stress loading on each fault have been calculated and plotted on Figure 3 as an average of the stress transferred to all elements. The calculated mean rates of loading are 0.00280 bars/yr for the Mt. Vettore fault, 0.00538 bars/yr for the Laga fault and 0.00679 bars/yr for the Norcia fault. The mean loading rate for the Mt. Vettore fault is the lowest of the three faults, but note that the elapsed time is the longest.

The accumulated interseismic Coulomb stress is heterogeneous with depth and distance along the fault as shown in Figure 4 which shows the total interseismic stress accumulated since the last earthquake on each individual fault. The highest magnitudes of interseismic Coulomb stress are seen at the base of the brittle faults, adjacent to the shear zones (which are not shown in Figure 4, but are shown in Figure 2). The Coulomb stress decreases up-dip of the brittle fault plane. Figure 4 shows that while the accumulated interseismic Coulomb stress in the upper portions of the faults are comparable between the Mt. Vettore, Laga and Norcia faults, close to the bottom of the brittle faults, there are marked differences in the accumulated stress between the different faults, due to the differences in elapsed time. It is assumed that any other forms of crustal and/or mantle deformation is constant across the three faults, due to their proximity. An important observation is that the Mt. Vettore fault has the highest

magnitude of stress from interseismic loading at the base of the brittle fault, whether the minimum (1316 years, 60 bars) or maximum elapsed time (4155 years, 200 bars) is considered.

3.2 Coseismic changes during the 2016-2017 seismic sequence

The modelled slip distributions and implied coseismic stress changes from the three largest earthquakes in the 2016-2017 sequence have been modelled and summed with the cumulative interseismic and coseismic stress transfer since 1349 A.D. (Figure 5). We show interseismic loading for the relatively long elapsed time on the Mt. Vettore fault as insets for each time step. Considering only the stresses that developed post 1349 A.D., prior to the onset of the sequence (Figure 5a), the regions of highest positive stress in the area of interest were on the Laga fault and the base of the Mt. Vettore fault. There were patches of positive stress evident on the Norcia fault, but the pattern is heterogeneous due to the occurrence of multiple historic earthquakes rupturing small portions of the fault (1730, 1830 [*Boncio et al.*, 2004]). The 24$^{th}$ August 2016 Mw 6.0 earthquake occurred on part of the northern end of the Laga fault, which was mostly positively stressed and also on the southern portion of the Mt. Vettore fault (as confirmed by field observations [*Livio et al.*, 2016], see Figure 5b). The southern termination of the rupture on the Laga fault coincides with the termination of the aftershock distribution from the 2009 L'Aquila sequence (see Figure 1). The northern termination of the rupture on the Mt. Vettore fault occurs at a prominent bend in the fault (B on Figure 5) that exhibited a strongly negative prior Coulomb stress pattern. The line of maximum curvature on the fault at this bend plunges to the SW, parallel to the slip-vector we measured at the surface from this earthquake (~220-240$^{o}$, Livio *et al.* [2016]). So this bend does not represent a

kinematic barrier to slip associated with the earthquake. Our results show that Coulomb stress is reduced by ~2 bars at this bend compared to adjacent fault sections; this may be an example of a stress barrier to rupture propagation (e.g. Steacy and McCloskey [1998]). Following the first earthquake, the northern portion of the Mt. Vettore fault was the most positively stressed region along the fault (Figure 5b). This is in part due to the positive stress transfer from the 1997 Umbria-Marche seismic sequence, but also in part due to the long interseismic loading since the last earthquake (see the inset showing interseismic stress since 4155 years BP). It is this highly-stressed patch on the northern portion of the Mt. Vettore fault that ruptured in the 26$^{th}$ October earthquake (Figure 5c); this portion is also called the Mt Bove fault [*Pizzi and Galadini*, 2009]. Note that this rupture terminated in the SE where Coulomb stress becomes negative across another bend in the fault (B' on Figure 5). We have no slip vector data (from surface observations) for this bend, but if the slip vector plunged SW parallel to the axis of maximum fault curvature at this bend then again, this would not have represented a kinematic barrier to slip during the earthquake. This is a sensible assumption given the variation of slip vectors on other normal faults [*Roberts*, 2007; *Faure Walker et al.*, 2010]. However, again, the marked decrease in stress makes this location another candidate for a stress barrier to rupture propagation. The 26$^{th}$ October earthquake increased the stress on the shallow portions of central section of the fault by 0.3-1 bars. Note the two thin stripes of positive stress located on two fault bends extending from 15 km depth almost to the surface in our model in the portion of the fault un-ruptured during Event 1 or 2 in the sequence (Figure 5c, B and B'). These highly-stressed patches plus the highly stressed base of the northern and southern portions of the Mt. Vettore fault were included in the ruptured fault surface in the 30$^{th}$ October Mw 6.5 earthquake with surface slip of up to

2.3 m [*Mildon et al.*, 2016b], as shown in Figure 5d. The 30th October event increased the stress on the Laga Fault, with the 18th January 2017 (Mw 5.1, 5.5, 5.4, 5.0) events occurring on a part of the fault that mostly shows positive Coulomb stress.

### 3.3 Stress history on the Mt. Vettore fault

A history of the mean stress across the Mt. Vettore fault is plotted in Figure 6, showing how the stress builds up interseismically and the fault experiences coseismic stress drops and increases from earthquakes occurring on surrounding faults. Only the largest and closest earthquakes to affect the Mt. Vettore fault are shown in this figure; stress transfer from other smaller or more distant earthquakes would be too small to be resolved on this scale. The stress drops from the 1328 A.D. Valnerina earthquake on the Norcia fault [*Boncio et al.*, 2004; *Guidoboni et al.*, 2007], the 1639 A.D. earthquake on the Laga fault [*Pace et al.*, 2002], the 1703 A.D. earthquake on the Norcia fault [*Blumetti*, 1995], the 1997 A.D. Colfiorito earthquake on the Mt Le Scalette fault and the 2009 A.D. L'Aquila earthquake on the Paganica fault are calculated and plotted. Note that the 1328 A.D. earthquake was excluded from previous calculations because it is before 1349 A.D. and probably less well-constrained, however for the purpose of highlighting the stress evolution of the Mt. Vettore fault, it has been included here. The absolute stress between 4155 years BP and 1328 A.D. is assumed to accumulate at the mean rate of interseismic loading (as shown in Figure 3) as there is no reliable information regarding coseismic stress transfer during earthquakes in this time period. Hence the absolute value of stress is subject to a number of assumptions as outlined herein and would be subject to variation if any of these assumptions were changed. The magnitude of the stress drops and increases are calculated independently. It is interesting to note the positive and

negative stress increases on the Mt. Vettore fault are in the range of 0-10 bars, with interseismic Coulomb stress changes are in the range of 0 to 60 bars or even 0 to 160 bars given the elapsed time on the Mt. Vettore fault. So it is unlikely that the interseismic loading will have been overwhelmed by stress decreases produced by earthquakes on faults across strike from the Mt. Vettore fault. This also implies that the major driving force causing earthquakes to occur is the long-term tectonic loading, and to a lesser degree the short-term coseismic Coulomb stress changes (although see Wedmore [2017] who shows that smaller faults are more sensitive to coseismic changes due to their relatively low slip-rates and hence interseismic loading rates).

### 3.4 January 2017 earthquakes

All four earthquakes with Mw>5.5 that occurred on the 18$^{th}$ January 2017 have been modelled. The Coulomb stress transfer from these events and the cumulative stress pattern as of the 19$^{th}$ January 2017 is shown in Figure 7. These earthquakes occurred in a region of mostly relatively high Coulomb stress (2 to >10 bars, see Figure 7a) on the Laga fault, with the exception of the third event, which occurred in a region of negative Coulomb stress. However, the second earthquake that occurred on this day was the largest event and may have increase the Coulomb stress in region that ruptured in the third event (along-strike). Also, given the short time duration between the second and third earthquakes (11 minutes), there may be some component of dynamic triggering involved. The coseismic stress transferred from these four earthquakes on the Laga fault has been added to the cumulative (interseismic and coseismic) stress since 1349 A.D. on this fault and is shown in Figure 7. The patches of zero stress are the regions of the fault that slipped; these should be considered as

minimum values of stress as we do not know if all the stress was relieved on these patches. Hence most of the Laga fault could be positively stressed at the present time.

## 4. Discussion

Coulomb stress transfer is routinely calculated following large earthquakes and used to infer the change in probability of the locations of aftershocks and subsequent mainshocks (e.g *Harris and Simpson* [1992]; *Reasenberg and Simpson* [1992]; Toda *et al.* [2012]; Pace *et al.* [2014]) and has been used for earthquake hazard assessment (e.g. Toda and Enescu [2011]). Many such studies do not include strike-variable faults, long earthquake histories from the historical record or the elapsed time since the last earthquake on receiver faults, however it has been shown for the 2009 L'Aquila earthquake that the magnitude of Coulomb stress transfer varies around bends in normal faults [*Mildon et al.*, 2016c] consistent with our results herein. Although valuable results can be obtained from planar fault geometries, such as the 1$^{st}$ order regional patterns of stress transfer, especially if they include interseismic loading and a large number of events from the historical catalogue, we argue that extra insights may be gained if we include strike-variable fault geometries and the known elapsed time on the faults of interest. This extra insight may help to explain the details of complicated seismic sequences like that in 2016-17 using Coulomb stress transfer (Figure 5).

We suggest that the sequence could not be fully explained if:

1) The whole historical sequence was not modelled, because stress heterogeneities arising from coseismic stress changes from historical earthquakes would not be evident on the Mt. Vettore fault;

2) The differences in elapsed time on the surrounding faults were not taken into account, as this helps to explain why the sequence began on the Laga fault and the continuation of the sequence on the Mt. Vettore fault;
3) The variable geometry was not modelled because it is this that creates a region of highly negative Coulomb stress in the bends on the fault and we hypothesise that these acted as a stress barriers to the ruptures of the 24$^{th}$ August and 26$^{th}$ October mainshocks (Figure 5b&c).

We also note that the relative geometry of the Norcia and Mt. Vettore faults affects the build up of Coulomb stress on the latter. During interseismic loading, the lower portion of the Mt. Vettore fault experiences its highest increase in Coulomb stress. When an earthquake occurs on the Norcia fault (e.g. the 1328 A.D. & 1703 A.D. earthquakes; Figure 6, 2. and 4.), the coseismic stress transferred onto the Mt. Vettore fault varies with depth. The upper portion of the fault experiences negative coseismic Coulomb stress transfer, whereas the lower portion experiences positive coseismic stress transfer. This positively reinforces the region of positive stress generated on the lower portion of the Mt. Vettore fault by interseismic loading even though the faults are located across strike. This is due to the horizontal across-strike distance between the two faults. The distance between the two faults is relatively constant in the southern portion of both faults, however in the northern region, the geometry of the Norcia fault changes (the strike changes from NNW-SSE to NW-SE) and the distance between the faults increases. This affects the stress transferred to the northern portion of the Mt. Vettore fault, as shown on Figure 6 for coseismic stress transfer from the 1703 A.D. earthquake (which likely ruptured the whole of the Norcia fault). This positively-stressed region at the northern end of the Mt. Vettore fault is clear in the

cumulative stress pattern in Figure 5a and shows the importance of the 1703 A.D. earthquake in contributing to the heterogeneous stress pattern on the Mt. Vettore fault. We hypothesise that this earthquake in particular caused the northern end of the Mt. Vettore fault to be more positively stressed and contributed to the stress pattern associated with the earthquakes of October 26th to occur on the northern portion of the Mt. Vettore fault, skipping the central section. This indicates that the relative geometry between faults is important, as well as the variations in geometry along single faults.

The southern 8 km of the Mt. Vettore fault ruptured during both Event 1 and 3 as evident from surface ruptures [*Livio et al.,* 2016] and INSAR results [*COMET*, 2016] and our own field observations [*Iezzi et al., in prep.; Mildon et al.,* 2016b]. At first sight this suggests that our assumption that the stress on a fault drops essentially to zero following an earthquake is incorrect, because the same patch ruptured twice within ~2 months. However, note that our models show that the base of the Mt. Vettore fault in its southernmost 8 km is positively stressed after the relatively shallow slip associated with the 24$^{th}$ August 2016 Mw 6.0 event (up to 30 bars if calculated from 1349 A.D.; up to 200 bars if calculated from 4155 years B.P.). Furthermore, after the 26$^{th}$ October, a region of highly positive Coulomb stress existed along the full 28 km length of the base of the fault with two apophyses of positive stress projecting to the surface at two prominent fault bends. This stress pattern appears to have contributed to the preparation of the Mt. Vettore fault for a Mw 6.5 earthquake with up to 2.3 m surface slip and a ~28 km rupture length [*Mildon et al.,* 2016b]. It may be that slip initiated at depth and was able to propagate up to near the surface via the positively stressed bends close to the central portion of the

fault, before spreading along strike to the SE and NE portions of the fault. These sections of the fault had already slipped in the 24th August and 26th October earthquakes, but the stress may or may not have dropped to zero during these events. This suggests that zero or low Coulomb stress patches on faults that have ruptured in recent events can be ruptured through subsequent earthquakes, if the pattern of positive stress, especially at the base of the fault, is extensive.

Overall this study shows that when the historical record, elapsed time and fault geometry are taken into account, the notion that the earthquakes occurred due to a seismic gap between the 1997 and 2009 earthquakes is perhaps correct, but oversimplified. As shown in Figure 6, the stress transferred to the Mt. Vettore fault from these two prior earthquakes was very small (~ 0.03 bars for the 1997 earthquake and ~ 0.01 bars for the 2009 earthquake) compared to the total accumulated stress on the fault (tens to hundreds of bars). The stress changes due to the other earthquakes shown in Figure 6 (1328 A.D., 1639 A.D. and 1703 A.D.) are of much greater magnitude (-0.93, 0.36 and -2.22 bars respectively) and therefore have more influence over the stress on the Mt. Vettore fault, despite being much longer ago (assuming the stresses have not dissipated over time). However, it is possible that some static stress may have dissipated over this short time period and therefore the stresses presented in this paper should be considered to be a maximum. We also note that the greatest magnitude of received coseismic stress change on the Mt. Vettore fault is negative and occurs when earthquakes occur on the Norcia fault, i.e. across strike. This shows that Coulomb stress drops play a more dominant role in delaying rupture than positive stress changes in preparing a receiver fault for rupture (see Wedmore *et al.*, [2015, submitted], Wedmore [2017] who first described this effect). Moreover, the

interseismic Coulomb stress loading must also be considered due to the high stress imparted to the base of the brittle faults. This emphasises the importance of including knowledge of the elapsed time on faults receiving stress (which can be thousands of years), even if knowledge of the coseismic stress changes are limited to a few hundred years by historical and paleoseismic records, as the interseismic stress may dominate over relatively small magnitude fluctuations produced by coseismic stress changes. Finally, the above calculations suggest that a large portion of the Laga fault is positively stressed after the 18th January earthquakes.

## 5. Conclusions

Using an approach to model Coulomb stress changes on strike-variable faults, we suggest that the central Apennines 2016-2017 seismic sequence on the Mt. Vettore and Laga faults can be explained by Coulomb stress transfer by including the coseismic changes from historical earthquakes and the interseismic loading for the elapsed time on the faults in the epicentral region. The first mainshock occurred on the Laga and Mt. Vettore faults due to regions of high Coulomb stress on both faults. The rupture length on the Laga fault appears to have been controlled by the extent of the aftershocks from the 2009 L'Aquila sequence (Figure 1). On the Mt. Vettore fault, the rupture appears to have been controlled by the presence of a fault bend creating a stress barrier. Following Event 1, the northern portion of the Mt. Vettore fault was the most positive due to the historical Coulomb stress transfer; hence the sequence jumped the central section. Four days later, in Event 3, the central section ruptured and the northern and southern sections re-ruptured due to high values of Coulomb stress along the entire base of the fault and two patches of positive stress extending almost to the surface on fault bends. The mean stress history on the Mt. Vettore fault

as shown in Figure 6 highlights the importance of considering the full historical catalogue of large earthquakes, as the coseismic changes from the most recent earthquakes in this example are negligible compared to previous stress drops and increases. Without including fault geometry, the historical catalogue and the elapsed time, we suggest that that the sequence of rupture locations with the jump to the north missing the central patch of the Mt. Vettore fault would be difficult to explain. It appears that it is only by including the fault geometry and coseismic stress changes since 1349 A.D. that generates stress heterogeneities, particularly on the Mt. Vettore fault, which can explain the distribution and limits of the mainshock ruptures. Finally, our calculations suggest that a large portion of the Laga fault is positively stressed after the 18th January earthquakes. Where future events occur will test the extent to which this approach can help inform seismic hazard analysis.

**Acknowledgements**

This study was funded by NERC Studentship NE/L501700/1, NERC Urgency Grant NE/P01660X/1 (EEFIT Reconnaissance Mission to the Amatrice, Italy, 24/09/2016 Earthquake) and NERC Standard Grant NE/I024127/1. The method to model strike-variable was developed during JSPS Short Term Fellowship (PE15776) undertaken by Zoe Mildon. Work was aided by a GBSF (Great Britain Saskawa Foundation) grant 4602 to Joanna Faure Walker.

**References**

Alessio, G. et al. (2009), Evidence for surface rupture associated with the Mw 6.3 L'Aquila earthquake sequence of April 2009 (central Italy), *Terra Nov.*, (April).

Blumetti, A. M. (1995), Neotectonic investigation of evidence of paleoseismicity in

the epicentral area of the January-February 1703, central Italy, earthquakes, *Perspect. Paleoseismology, Assoc. Eng. Geol. Bull., Special Pu*, 83–100.

Boncio, P., G. Lavecchia, and B. Pace (2004), Defining a model of 3D seismogenic sources for Seismic Hazard Assessment applications: The case of central Apennines (Italy), *J. Seismol.*, *8*(3), 407–425, doi:10.1023/B:JOSE.0000038449.78801.05.

Cello, G., G. Deiana, P. Mangano, S. Mazzoli, E. Tondi, L. Ferreli, L. Maschio, A. M. Michetti, L. Serva, and E. Vittori (1998), Evidence for surface faulting during the September 26, 1997, Colfiorito (central Italy) earthquakes, *J. Earthq. Eng.*, *2*(2), 303–324, doi:10.1080/13632469809350324.

Chiaraluce, L., C. Chiarabba, P. De Gori, R. Di Stefano, L. Improta, D. Piccinini, A. Schlagenhauf, P. Traversa, L. Valoroso, and C. Voisin (2010), The 2009 L'Aquila (Central Italy) Seismic Sequence., *Boll. di Geofis. Teor. e Appl.*, 1–29.

COMET (2016), Apennines earthquakes and aftershocks, Italy, *COMET blog*. [online] Available from: http://comet.nerc.ac.uk/latest-earthquakes-and-eruptions/apennines-earthquakes-aftershocks-italy/ (Accessed 5 December 2016)

Cowie, P. A., C. H. Scholz, G. P. Roberts, J. P. Faure Walker, and P. Steer (2013), Viscous roots of active seismogenic faults revealed by geologic slip rate variations, *Nat. Geosci.*, *6.12*(November), 1036–1040, doi:10.1038/ngeo1991.

Deng, J., and L. R. Sykes (1997), Evolution of the stress field in southern California and triggering of moderate-size earthquakes: A 200-year perspective, *J. Geophys. Res.*, *102*, 9859–9886.

Faure Walker, J. P., G. P. Roberts, P. A. Cowie, I. D. Papanikolaou, P. R. Sammonds, A. M. Michetti, and R. J. Phillips (2009), Horizontal strain-rates and throw-rates across breached relay zones, central Italy: Implications for the preservation of

throw deficits at points of normal fault linkage, *J. Struct. Geol.*, *31*(10), 1145–1160, doi:10.1016/j.jsg.2009.06.011.

Faure Walker, J. P., G. P. Roberts, P. R. Sammonds, and P. A. Cowie (2010), Comparison of earthquake strains over 10 2 and 10 4 year timescales: Insights into variability in the seismic cycle in the central Apennines, Italy, *J. Geophys. Res.*, *115*(B10), B10418, doi:10.1029/2009JB006462.

Faure Walker, J. P., G. P. Roberts, P. A. Cowie, I. D. Papanikolaou, A. M. Michetti, P. R. Sammonds, M. Wilkinson, K. J. W. McCaffrey, and R. J. Phillips (2012), Relationship between topography, rates of extension and mantle dynamics in the actively-extending Italian Apennines, *Earth Planet. Sci. Lett.*, *325–326*, 76–84, doi:10.1016/j.epsl.2012.01.028.

Galadini, F., and P. Galli (2000), Active Tectonics in the Central Apennines (Italy)–Input Data for Seismic Hazard Assessment, *Nat. Hazards*, *22*, 225–270.

Galadini, F., and P. Galli (2003), Paleoseismology of silent faults in the Central Apennines (Italy): the Mt . Vettore and Laga Mts . faults, *Ann. Geophyics*, *46*(October), 815–836.

Galli, P., F. Galadini, and F. Calzoni (2005), Surface faulting in Norcia (central Italy): a "paleoseismological perspective," *Tectonophysics*, *403*(1–4), 117–130, doi:10.1016/j.tecto.2005.04.003.

Galli, P., F. Galadini, and D. Pantosti (2008), Twenty years of paleoseismology in Italy, *Earth-Science Rev.*, *88*(1–2), 89–117, doi:10.1016/j.earscirev.2008.01.001.

Guidoboni, E., G. Ferrari, D. Mariotti, A. Comastri, G. Tarabusi, and G. Valensise (2007), CFTI4Med, Catalogue of Strong Earthquakes in Italy (461B.C.-1997) and Mediterranean Area (760B.C.-1500), *INGV-SGA*. [online] Available from: http://storing.ingv.it/cfti4med/

Harris, R. A., and R. W. Simpson (1992), Changes in static stress on southern California faults after the 1992 Landers earthquake, *Nature*, *360*(6401), 251–254, doi:10.1038/360251a0.

INGV working group (2016), *Second summary report of the Ml 6.0 Amatrice earthquake of August 24, 2016 (central Italy).*

Lin, J., and R. S. Stein (2004), Stress triggering in thrust and subduction earthquakes and stress interaction between the southern San Andreas and nearby thrust and strike-slip faults, *J. Geophys. Res.*, *109*(B2), B02303, doi:10.1029/2003JB002607.

Livio, F. et al. (2016), Surface faulting during the August 24, 2016, Central Italy earthquake (Mw 6.0): preliminary results, *Ann. Geophyics*, (11), 1–8.

Michetti, A. M., F. Brunamonte, L. Serva, and E. Vittori (1996), Trench investigation of the 1915 Fucino earthquake fault scarps (Abruzzo, central Italy): Geological evidence of large historical events., *J. Geophys. Res.*, *101*, 5921–5936.

Mildon, Z. K., G. P. Roberts, J. P. Faure Walker, L. Wedmore, and K. J. W. McCaffrey (2016a), Active normal faulting during the 1997 seismic sequence in Colfiorito, Umbria: Did slip propagate to the surface?, *J. Struct. Geol.*, doi:10.1016/j.jsg.2016.08.011.

Mildon, Z. K. et al. (2016b), Detailed surface rupture geometry from the 2016 Amatrice earthquake (24th August and 30th October), in *AGU Fall Meeting 12th-16th December 2016*, San Francisco.

Mildon, Z. K., S. Toda, J. P. Faure Walker, and G. P. Roberts (2016c), Evaluating models of Coulomb stress transfer: Is variable fault geometry important?, *Geophys. Res. Lett.*, 1–8, doi:10.1002/2016GL071128.

Morewood, N. C., and G. P. Roberts (2000), The geometry, kinematics and rates of

deformation within an en echelon normal fault segment boundary, central Italy, *J. Struct. Geol.*, *22*(8), 1027–1047, doi:10.1016/S0191-8141(00)00030-4.

Nalbant, S. S., A. Hubert, and G. C. P. King (1998), Stress coupling between earthquakes in northwest Turkey and the north Aegean Sea, *J. Geophys. Res.*, *103*(B10), 24469–24486.

Nostro, C., L. Chiaraluce, M. Cocco, D. Baumont, and O. Scotti (2005), Coulomb stress changes caused by repeated normal faulting earthquakes during the 1997 Umbria-Marche (central Italy) seismic sequence, *J. Geophys. Res.*, *110*(B5), B05S20, doi:10.1029/2004JB003386.

Pace, B., L. Peruzza, G. Lavecchia, and P. Boncio (2002), Seismogenic sources in Central Italy: from causes to effects, *Mem. della Soc. Geol. Ital.*, *57*, 419–429.

Pace, B., L. Peruzza, G. Lavecchia, and P. Boncio (2006), Layered Seismogenic Source Model and Probabilistic Seismic-Hazard Analyses in Central Italy, *Bull. Seismol. Soc. Am.*, *96*(1), 107–132, doi:10.1785/0120040231.

Pace, B., G. M. Bocchini, and P. Boncio (2014), Do static stress changes of a moderate-magnitude earthquake significantly modify the regional seismic hazard? Hints from the L'Aquila 2009 normal-faulting earthquake (Mw 6.3, central Italy), *Terra Nov.*, *26*(6), 430–439, doi:10.1111/ter.12117.

Papanikolaou, I. D., and G. P. Roberts (2007), Geometry, kinematics and deformation rates along the active normal fault system in the southern Apennines: Implications for fault growth, *J. Struct. Geol.*, *29*(1), 166–188, doi:10.1016/j.jsg.2006.07.009.

Papanikolaou, I. D., G. P. Roberts, and A. M. Michetti (2005), Fault scarps and deformation rates in Lazio–Abruzzo, Central Italy: Comparison between geological fault slip-rate and GPS data, *Tectonophysics*, *408*(1–4), 147–176,

doi:10.1016/j.tecto.2005.05.043.

Peruzza, L., R. Gee, B. Pace, G. P. Roberts, O. Scotti, F. Visini, L. Benedetti, and M. Pagani (2016), PSHA after a strong earthquake: hints for the recovery, *Ann. Geophys.*, *59*, 1–9.

Pizzi, A., and F. Galadini (2009), Pre-existing cross-structures and active fault segmentation in the northern-central Apennines (Italy), *Tectonophysics*, *476*(1–2), 304–319, doi:10.1016/j.tecto.2009.03.018.

Reasenberg, P. a, and R. W. Simpson (1992), Response of regional seismicity to the static stress change produced by the loma prieta earthquake., *Science*, *255*(5052), 1687–1690, doi:10.1126/science.255.5052.1687.

Roberts, G. P. (2007), Fault orientation variations along the strike of active normal fault systems in Italy and Greece: Implications for predicting the orientations of subseismic-resolution faults in hydrocarbon reservoirs, *Am. Assoc. Pet. Geol. Bull.*, *91*(1), 1–20, doi:10.1306/08300605146.

Roberts, G. P. (2008), Visualisation of active normal fault scarps in the Apennines, Italy: a key to assessment of tectonic strain release and earthquake rupture, *J. Virtual Explor.*, *29*(4), doi:10.3809/jvirtex.2008.00197.

Roberts, G. P., and A. M. Michetti (2004), Spatial and temporal variations in growth rates along active normal fault systems: an example from The Lazio–Abruzzo Apennines, central Italy, *J. Struct. Geol.*, *26*(2), 339–376, doi:10.1016/S0191-8141(03)00103-2.

Rydelek, P. A., and I. S. Sacks (1999), Large earthquake occurrence affected by small stress changes, *Bull. Seismol. Soc. Am.*, *89*(3), 822–828, doi:10.1144/GSL.SP.2001.184.01.06.

Steacy, S. J., and J. McCloskey (1998), What controls an earthquake's size? Results

from a heterogeneous cellular automaton, *Geophys. J. Int.*, *133*(1), F11–F14, doi:10.1046/j.1365-246X.1998.1331548.x.

Stein, R., and V. Sevilgen (2016), Italy earthquake leaves seismic gaps that were last filled by three large earthquakes in 1703, *Temblor blog*. [online] Available from: http://temblor.net/earthquake-insights/gaps-persist-beyond-ends-m6-2-rieti-italy-earthquake-progressive-sequence-large-shocks-struck-1703-1216/ (Accessed 29 August 2016)

Toda, S., and B. Enescu (2011), Rate/state Coulomb stress transfer model for the CSEP Japan seismicity forecast, *Earth, Planets Sp.*, *63*(3), 171–185, doi:10.5047/eps.2011.01.004.

Toda, S., R. S. Stein, K. Richards-Dinger, and S. B. Bozkurt (2005), Forecasting the evolution of seismicity in southern California: Animations built on earthquake stress transfer, *J. Geophys. Res.*, *110*(B5), B05S16, doi:10.1029/2004JB003415.

Toda, S., R. S. Stein, G. C. Beroza, and D. Marsan (2012), Aftershocks halted by static stress shadows, *Nat. Geosci.*, *5*(6), 410–413, doi:10.1038/ngeo1465.

Valoroso, L., L. Chiaraluce, D. Piccinini, R. Di Stefano, D. Schaff, and F. Waldhauser (2013), Radiography of a normal fault system by 64,000 high-precision earthquake locations: The 2009 L'Aquila (central Italy) case study, *J. Geophys. Res. Solid Earth*, *118*(3), 1156–1176, doi:10.1002/jgrb.50130.

Vittori, E. et al. (2000), Ground effects and surface faulting in the September-October 1997 Umbria-Marche (central Italy) seismic sequence, *J. Geodyn.*, *29*, 535–564.

Walters, R. J., J. R. Elliott, N. D'Agostino, P. C. England, I. Hunstad, J. A. Jackson, B. E. Parsons, R. J. Phillips, and G. P. Roberts (2009), The 2009 L'Aquila earthquake (central Italy): A source mechanism and implications for seismic hazard, *Geophys. Res. Lett.*, *36*(17), 2–7, doi:10.1029/2009GL039337.

Wedmore, L. N. J. (2017), Fault interaction processes and continental extension in the central Apennines, Italy, University College London.

Wedmore, L. N. J., J. P. Faure Walker, G. P. Roberts, K. J. W. McCaffrey, P. R. Sammonds, P. A. Cowie, and L. C. Gregory (2015), Coulomb stress changes over a 660-year period in central Italy: Implications for understanding fault interactions and earthquake occurrence, in *AGU Fall Meeting 14th-18th December 2015*.

Wedmore, L. N. J., J. P. Faure Walker, G. P. Roberts, P. R. Sammonds, K. J. W. McCaffrey, and P. A. Cowie (n.d.), A 667-year record of co-seismic and interseismic Coulomb stress changes in central Italy reveals the role of fault interaction in controlling irregular earthquake recurrence intervals, *Submitt. to J. Geophys. Res. Solid Earth*.

Wells, D. L., and K. J. Coppersmith (1994), New Empirical Relationships among Magnitude, Rupture Length, Rupture Width, Rupture Area, and Surface Displacement, *Bull. Seismol. Soc. Am.*, *84*(4), 974–1002.

Wilkinson, M. et al. (2015), Slip distributions on active normal faults measured from LiDAR and field mapping of geomorphic offsets: an example from L'Aquila, Italy, and implications for modelling seismic moment release, *Geomorphology*, *237*, 130–141, doi:10.1016/j.geomorph.2014.04.026.

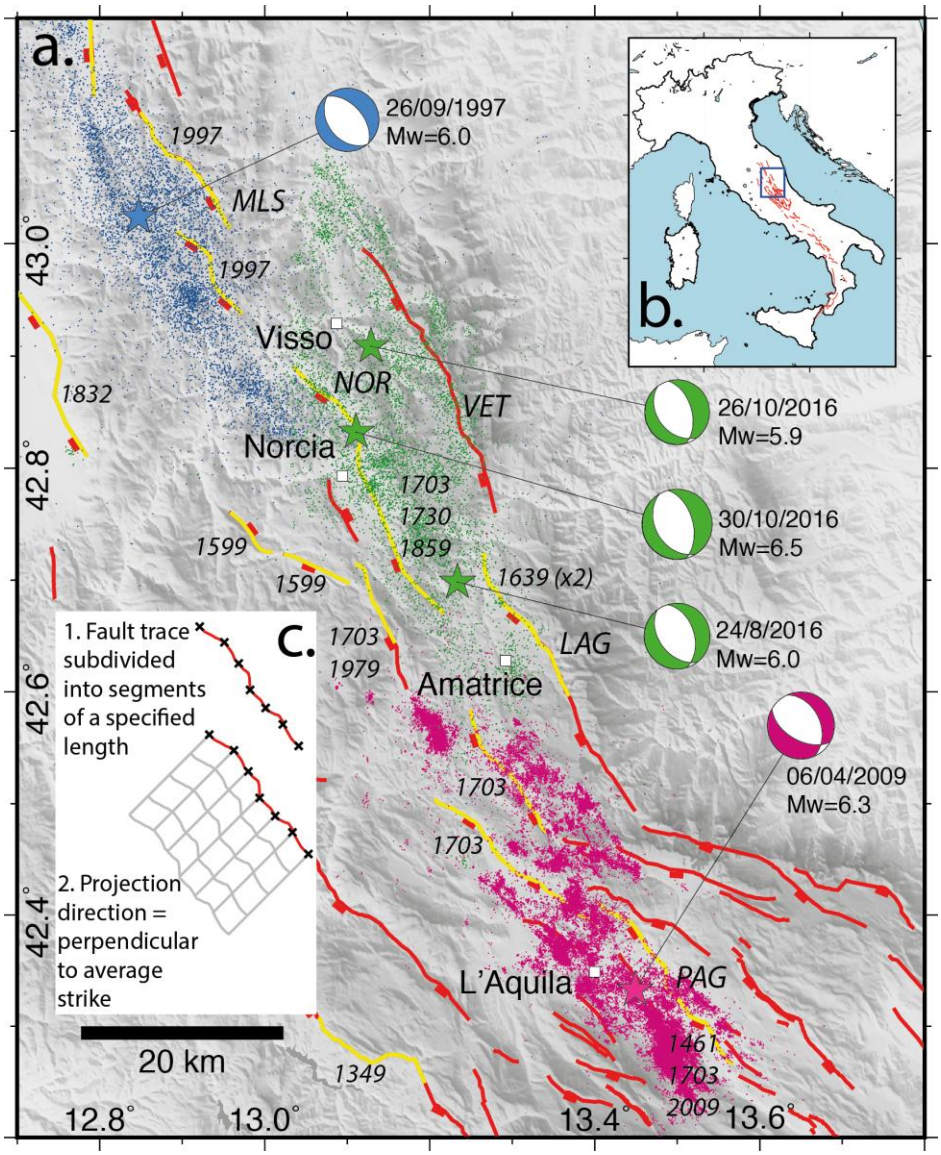


Figure 1- a. Map of the region of the 2016 seismic sequence, central Italy. Red lines indicate the locations of active faults; tick marks are on the hanging wall. The location of historical earthquake ruptures are shown in yellow and labelled with the year of the earthquake. Earthquakes >M2 from the last three earthquake sequences are shown. The 1997 Umbria-Marche seismic sequence is shown in blue, mainshock marked with a blue star, location from the INGV. The 2009 L'Aquila aftershocks are shown in pink, mainshock marked as a pink star, from Valoroso *et al.*, [2013]. The 2016 Amatrice sequence is shown in green, with the three mainshocks marked as green

stars, locations from the INGV. Focal mechanisms and magnitudes are from the CMT catalogue. Faults discussed in the text are labelled; VET-Mt. Vettore fault, NOR-Norcia fault, LAG-Laga fault, PAG-Paganica fault, MLS-Mt Le Scalette fault. b. The location of a. within Italy. The extent of a. is marked by the blue box. c. Method of generating the 3-D strike-variable faults for use in Coulomb 3.4. 1. Fault trace is subdivided into segments of a specified length. For the examples shown in this paper, the specified length is 1 km. 2. Using an assigned projection direction that is perpendicular to the mean strike of the fault, the segment boundaries (shown as crosses) are projected to depth.

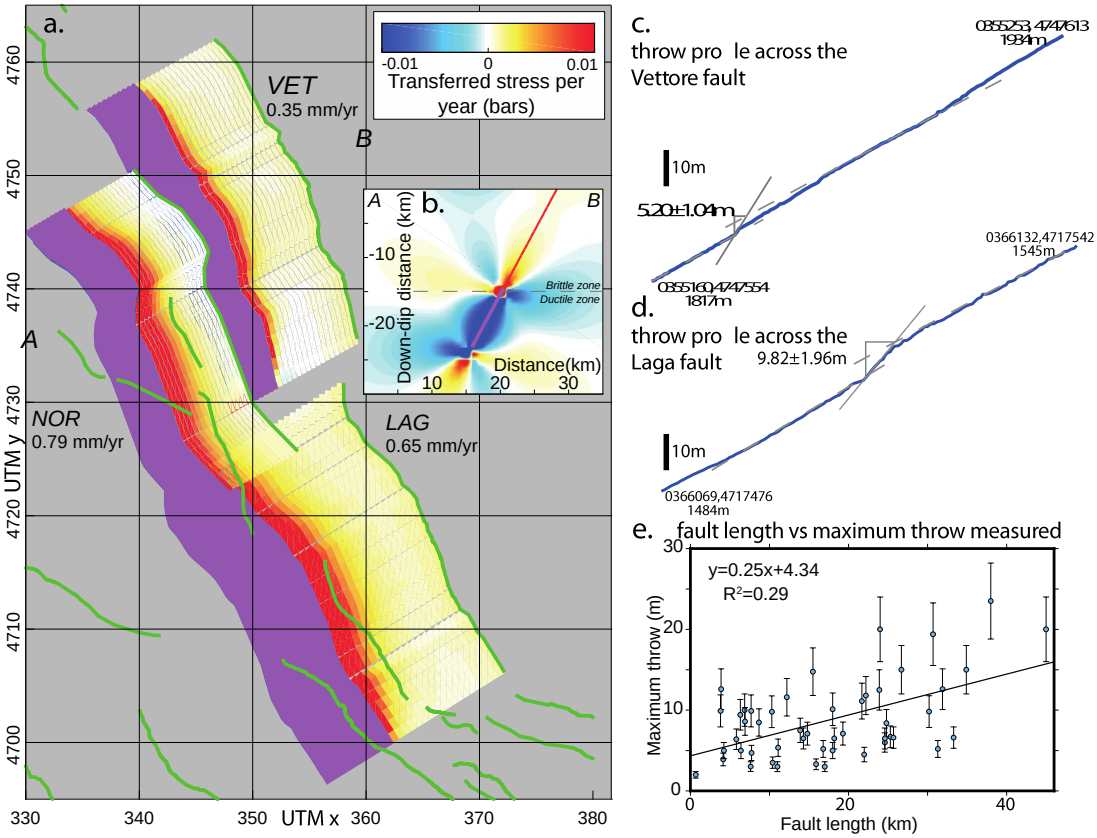


Figure 2- a.) One year of interseismic loading on the Mt. Vettore, Laga and Norcia faults. The maximum stress transferred to a single brittle element is 0.1 bar (at the base of the Norcia fault). The traces of other active faults are shown in green. The Holocene slip rates are also given for each fault. b.) a cross section across the Mt. Vettore fault from A to B (not including the Norcia fault), the shear zone in the ductile zone is highlighted in purple. This shows how positive stress is transferred to the upper brittle part of the active fault. Topographic profiles of the c.) Mt. Vettore fault and d.) Laga fault show how the slip rates are derived. These profiles are constructed using a metre ruler and a clinometer and noting the location of the upper slope (mid-blue dashed line), degraded fault plane, preserved free face and lower slope (green dashed line). UTM coordinates and heights of the start and end points are given. e.) graph to show the relationship between the lengths of active faults in the

central Apennines and the maximum throw measured along each fault. This relationship is used to assign a throw to the Norcia fault as this fault is poorly exposed in the field, so topographic profiles of the Holocene scarp cannot be taken.

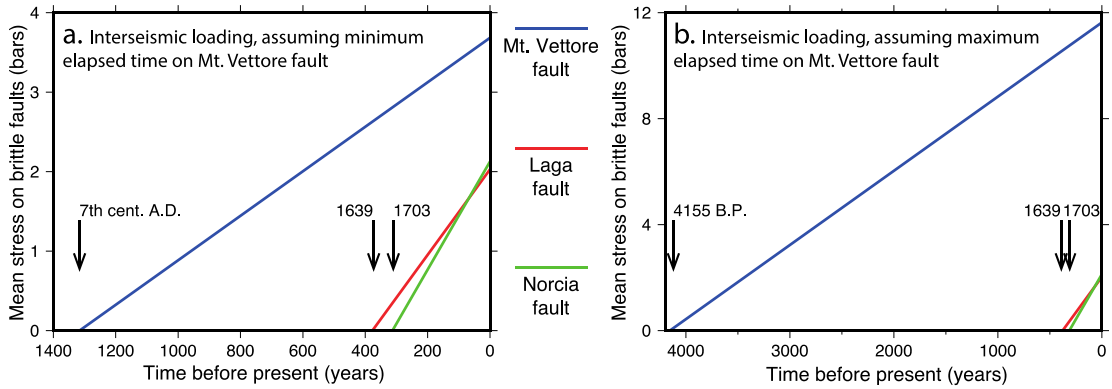


Figure 3- Mean interseismic loading rates on the Mt. Vettore, Laga and Norcia faults, from the time of the last earthquake on each of the respective faults. The last earthquake on the Laga and Norcia faults are known from the historical record as 1639 [*Boncio et al.*, 2004; *Guidoboni et al.*, 2007] and 1703 [*Blumetti*, 1995] respectively. The last earthquake on the Mt. Vettore fault is given as a range of dates in Galadini and Galli [2003], from 4155 years BP to 7$^{th}$ century AD. a.) assuming the minimum elapsed time on the Mt. Vettore fault, b.) assuming the maximum elapsed time on the Mt. Vettore fault. In each case, the magnitude of interseismic loading is highest on the Mt. Vettore fault due to a longer elapsed time relative to the Norcia and Laga faults, despite a lower loading rate. These figures show that the mean stress on the faults in 2016 was 2 bars for the Laga fault, 2.1 bars for the Norcia fault and 3.7-11.6 bars for the Vettore fault (due to the range in elapsed time).

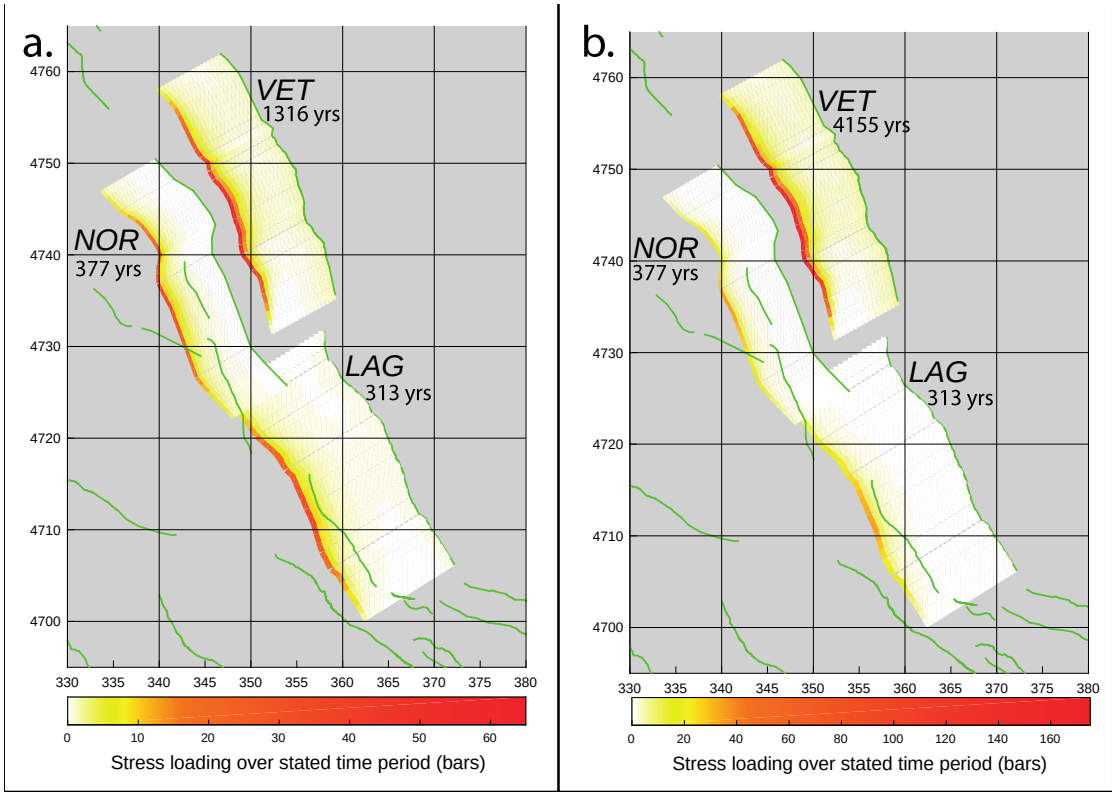


Figure 4- Interseismic stress accumulated on the Mt. Vettore (VET), Laga (LAG) and Norcia (NOR) faults since the last earthquake on each fault. The brittle portions of the faults are shown; the shear zone at 15-24 km depth is not shown. Other active surface fault traces are shown by the green traces. This assumes the stress dropped to zero during the last earthquake. a.) minimum elapsed time on the Mt. Vettore fault and b.) maximum elapsed time on the Mt. Vettore fault.

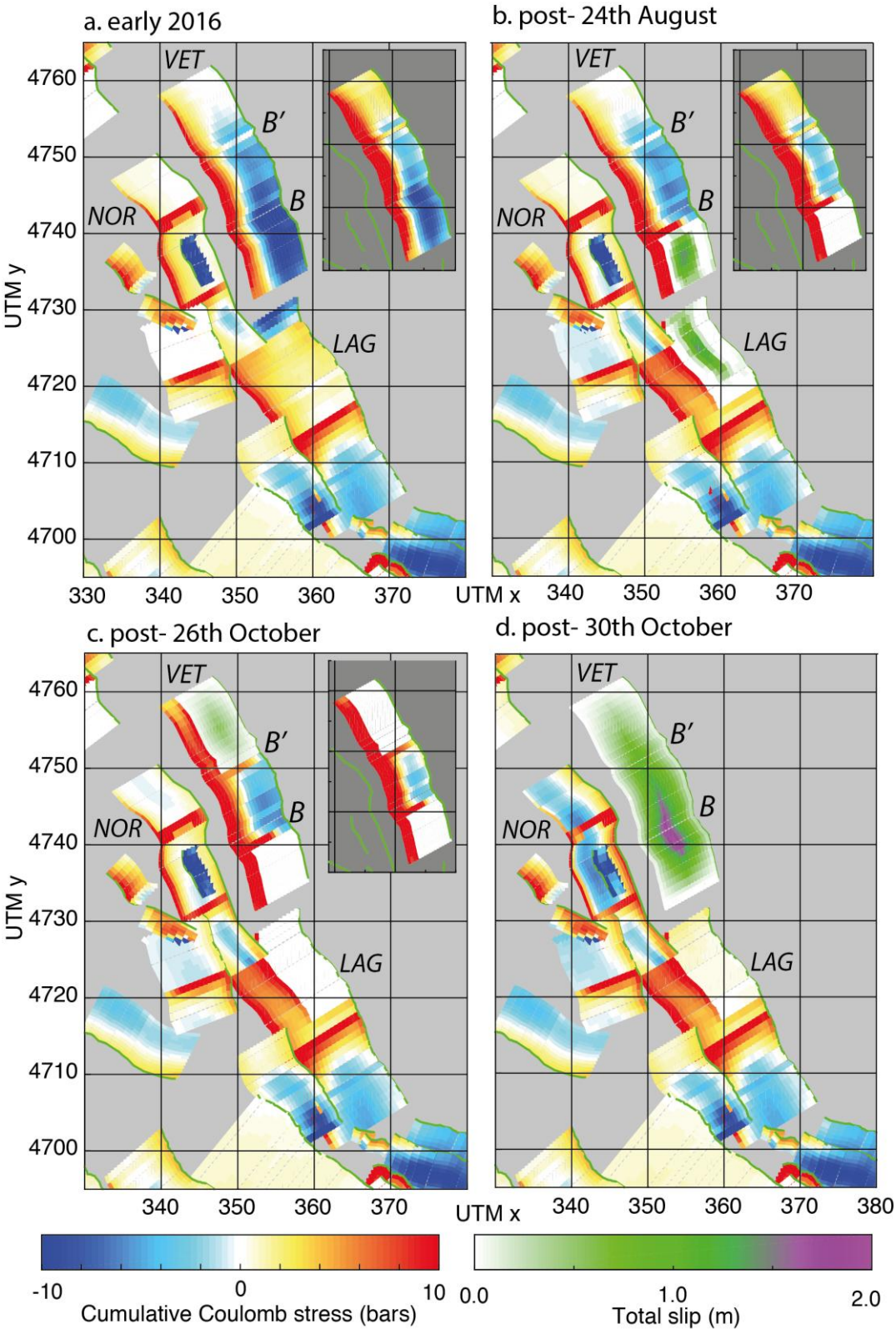


Figure 5- Changes in cumulative (interseismic and coseismic stress) throughout the 2016 seismic sequence. This includes all interseismic and coseismic loading from 1349 to the present day. Stress is assumed to be zero in 1349 and drops to zero

following each earthquake; this is the minimum value. The insets show the stress on the Mt. Vettore fault including the interseismic loading from 4155yr BP to 1349. Coseismic slip for each of the three mainshocks of the sequence is also shown in b-d. *B* and *B'* mark the locations of bends that exhibits a stress pattern of particular interest which is discussed in the text. The Norcia (NOR), Mt. Vettore (VET) and Lag (LAG) faults are marked. a.) cumulative stress prior to the 2016 seismic sequence. b.) cumulative stress after the first mainshock on the 24$^{th}$ August. The slip distribution used is published by the INGV [*INGV working group*, 2016]. c.) cumulative stress after the second mainshock on the 26$^{th}$ October. The slip distribution used is a simple bulls-eye and the length of fault rupture is determined by the INSAR. d.) cumulative stress after the third mainshock on the 30$^{th}$ October. The slip distribution used is a simple bulls-eye skewed to the south east (in agreement with surface offsets and INSAR).

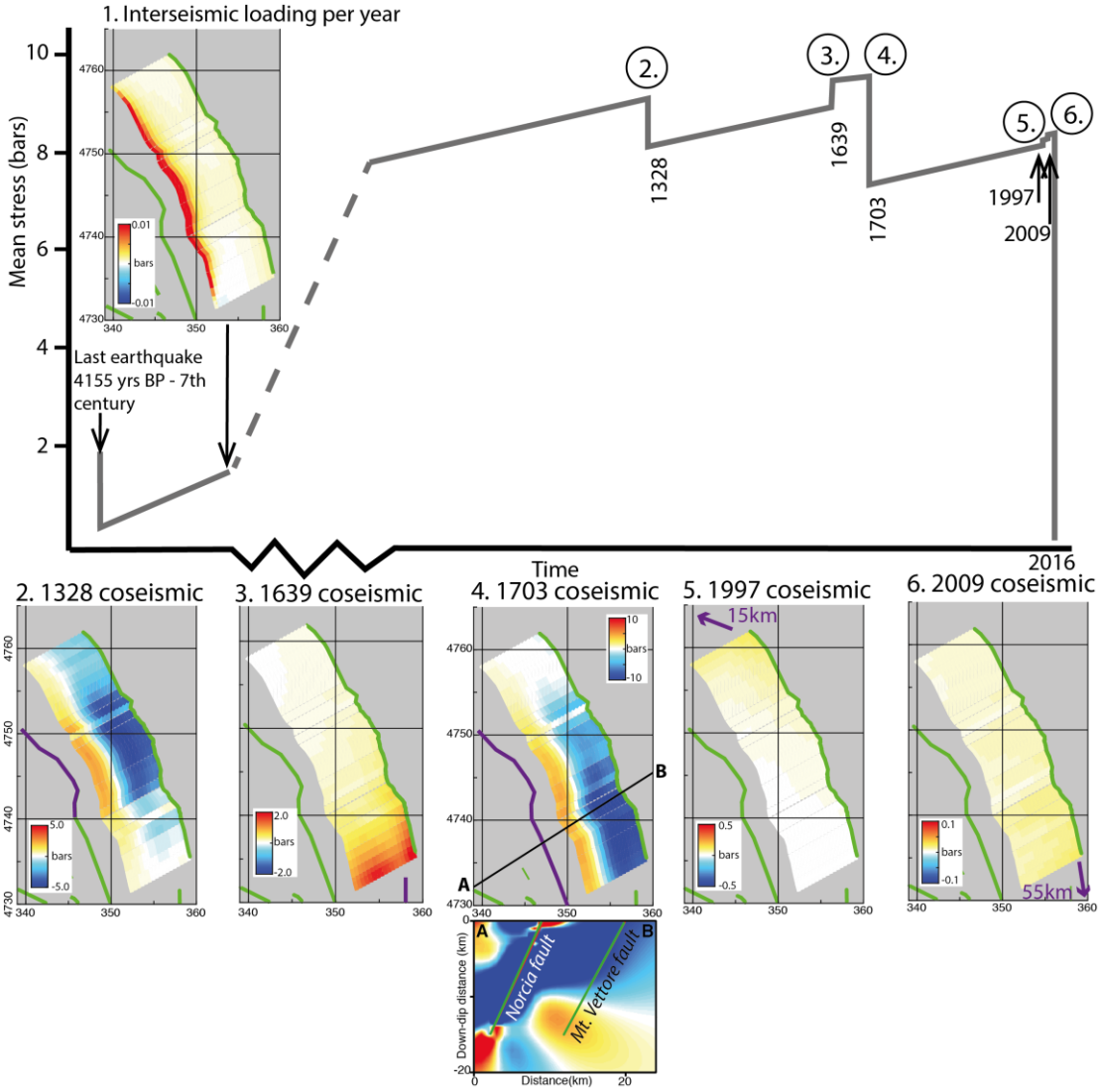


Figure 6- Mean stress history of the Mt. Vettore fault. The date of the last earthquake is between 4155yr BP and 7$^{th}$ century AD, the absolute magnitude of stress calculated uses 4155 years as the elapsed time. Historical earthquakes with magnitude >6 close to the Mt. Vettore fault are modelled and included. The location of the historical earthquake is shown as a purple trace along the responsible fault or an arrow indicating the direction and distance. The green lines show the locations of active faults around the Mt. Vettore fault. The magnitudes of the coseismic stress drops/increases are independent of the elapsed time on the Mt. Vettore fault. Selected Coulomb stress models are shown, note the differences in scale. 1. Interseismic loading rate, 2. Coseismic stress drop from the 1328 earthquake, which occurred on

the Norcia fault [*Boncio et al.*, 2004]. 3. Sum of coseismic stress increase from two earthquakes in 1639 on the Laga fault. 4. Coseismic stress drop from the 1703 earthquake, which occurred on the Norcia fault. A cross-section across the Norcia and Mt. Vettore faults shows the region of positive coseismic stress transferred to the base of the Mt. Vettore fault. 5. Coseismic stress increase from the 1997 Colfiorito earthquake that occurred on the Mt Le Scalette fault. 6. Coseismic stress increase from the 2009 L'Aquila earthquake on the Paganica fault. This shows that the coseismic stress loading from the two most recent earthquakes are minor relative to prior historical events.

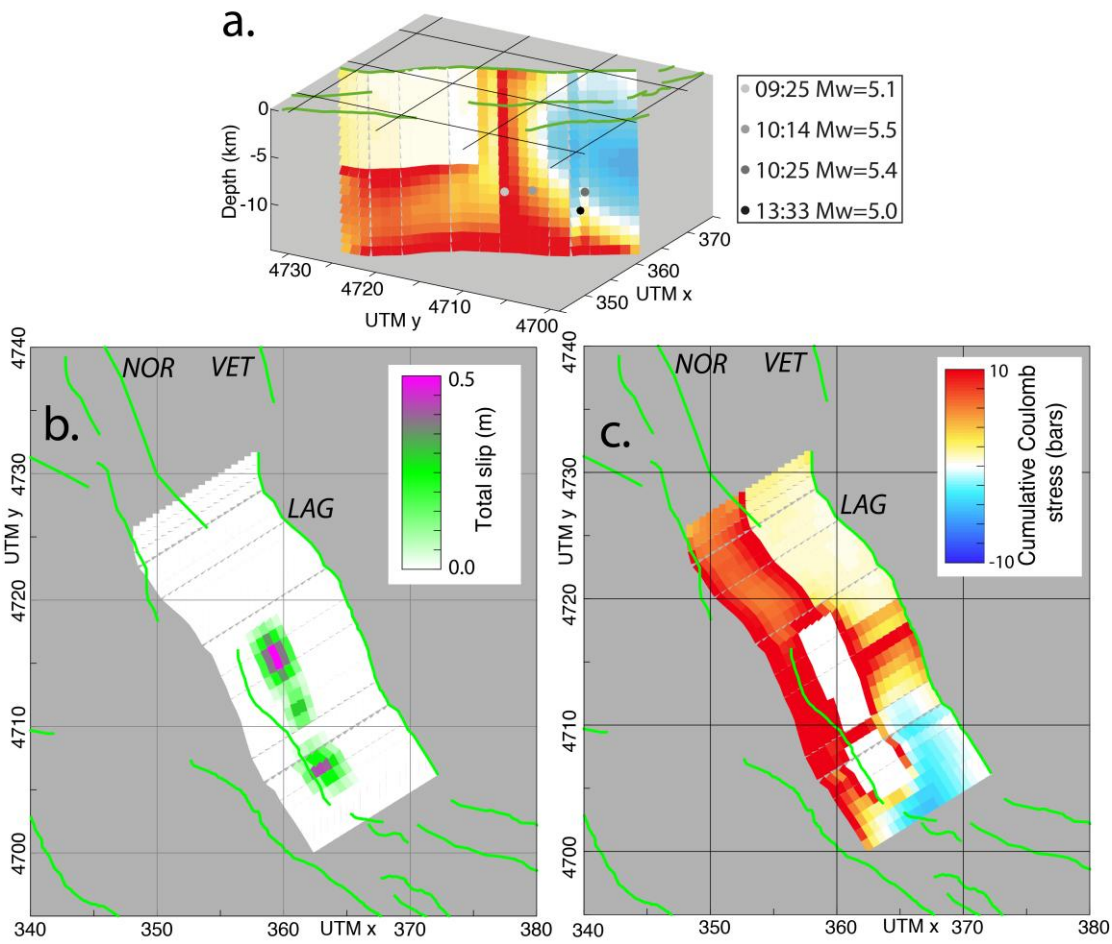


Figure 7- a.) The cumulative stress on the Laga fault following the 30th October earthquake, with the earthquakes of the 18th January 2017 plotted (locations from the INGV). The locations are coloured coded with a grey scale to indicate the order in which they occurred. The earthquake that occurred in the negatively stressed region occurred 11 minutes after the largest earthquake to occur on this day. Therefore there may have been additional positive static Coulomb stress transferred to the location of the third earthquake, or dynamic triggering may have occurred. b.) the slip distribution of the four Mw>5.0 earthquakes on the 18th January 2017. Note that two of the slip patches overlap. c.) Cumulative interseismic and coseismic stress from 1349 to 19th January 2017 on the Laga fault. The traces of active faults are marked in green and the Norcia (NOR), Mt Vettore (VET) and Laga (LAG) faults are marked. The regions that slipped during the four earthquakes on the 18th January are show by

black dashed lines, in these regions the stress is displayed as zero, however this is a minimum as it is not known whether all the stress has been relieved.